Journal of Hazardous Materials 169 (2009) 297–301

Contents lists available at ScienceDirect

Journal of Hazardous Materials

journal homepage: www.elsevier.com/locate/jhazmat

Photocatalytic decouloration of malachite green dye by application of TiO_2 nanotubes

Alexandre G.S. Prado*, Leonardo L. Costa

Instituto de Química, Universidade de Brasília, Caixa Postal 4478, 70904-970 Brasília, Distrito Federal, Brazil

ARTICLE INFO

Article history:
Received 15 November 2008
Received in revised form 29 January 2009
Accepted 20 March 2009
Available online 27 March 2009

Keywords:
Malachite green dye
Nanotubes
Photodegradation

ABSTRACT

The nanotubes of titania were synthesized in a hydrothermal system and characterized by scanning electronic microscopy (SEM), FT-IR, FT-Raman, and surface charge density by surface area analyzer. These nanomaterials were applied to photocatalyse malachite green dye degradation. Photodegradation capacity of TiO_2 nanotubes was compared to TiO_2 anatase photoactivity. Malachite dye was completely degraded in 75 and 105 min of reaction photocatalysed by TiO_2 nanotubes and TiO_2 anatase, respectively. Catalysts displayed high photodegradation activity at pH 4. TiO_2 nanotubes were easily recycled whereas the reuse of TiO_2 anatase was not effective. Nanotubes maintained 80% of their activity after 10 catalytic cycles and TiO_2 anatase presented only 8% of its activity after 10 cycles.

1. Introduction

High amount of unconsumed dyes produced by textile and printing industries are discharged into the waters every day. The presence of dyes and pigments in water causes considerable damage to the aquatic environment [1–3]. These contaminants result in high chemical oxygen demand (COD), high biochemical oxygen demand (BOD), toxicity, bad smell, and mainly, are responsible for the coloration of wastewaters [3,4]. Even at very low concentrations, the color of this kind of contaminants can be recognized, because the presence of dyes in water is highly visible. This effect is undesirable because the color blocks the sunlight access to aquatic flora and fauna, and it reduces the photosynthetic action within the ecosystem [5,6]. Among many dyes that are applied in manufacture products, malachite green must be highlighted. This dye has been used as a food coloring additive, as a dye for silk, jute, leather, wool, cotton and paper [7,8]. Moreover, this compound has also been used as a medical disinfectant, antihelminthic, as well as, in aquaculture as a fungicide and antiseptic [9,10].

The application of malachite green in aquaculture dates back 1933, due to its high effect against protozoal and fungal infections [11,12]. However, the use of malachite green has been contested due to the effects on the reproductive and immune systems and its potential genotoxic and carcinogenic effects. Thus, its use in aquaculture has not been authorized in Europe and in the United States of America [13]. Many processes have extensively applied the treatment of dye-containing wastewater such as: incineration, biological treatment, ozonation, adsorption on solid phases [14–17]. However, these procedures have some limitations. The incineration can produce toxic volatiles; biological treatment demands long periods of treatment and bad smell; ozonation presents a short half-life, ozone stability is affected by the presence of salts, pH, and temperature and the adsorption results in phase transference of contaminant, not degrading the contaminant and producing sludge [14–17].

In this way, the heterogeneous photocatalysis becomes an elegant alternative for dye degradation. This technique presents many advantages over conventional technologies such as the dye degradation into innocuous final products [18,19].

Many photocatalysts have been used to degrade organic pollutants such as ZnO, Nb_2O_5, TiO_2. Among these catalysts, TiO_2 is highlighted because of its high catalytic efficiency, high chemical stability, low cost and toxicity. On the other hand, TiO_2 suspension in water presents a hydrocolloid with a high stability, which makes difficult the separation of this catalyst from water. Consequently, the recuperation and re-application of this catalyst in other photodegradation reactions becomes hard and with a low efficiency [18–20].

In order to avoid this difficult recuperation, the TiO_2 nanotubes were synthesized, characterized and applied to the photodegradation of malachite green dye. Recycling studies were followed and compared to traditional TiO_2 anatase photocatalyst in order to demonstrate the advantages of nanostructured TiO_2 in photocatalysis.

* Corresponding author. Fax: +55 61 32734149.
E-mail addresses: agspradus@gmail.com, agsprado@unb.br (A.G.S. Prado).

0304-3894/$ – see front matter © 2009 Published by Elsevier B.V.
doi:10.1016/j.jhazmat.2009.03.076

2. Experimental

2.1. Chemicals

TiO_2 (anatase) (Acros), malachite green dye (Vetec), NaOH (Sigma), NaCl (Vetec), NaOH (Vetec) and HNO_3 (Vetec) were used without further purification.

2.2. TiO_2 nanotubes synthesis

The titania nanotube was synthesized by a hydrothermal reaction between NaOH solution and TiO_2 anatase. A total of 8 g of TiO_2 was suspended in 100 mL of 10 mol L^{-1} NaOH aqueous solution. This suspension was stirred during 15 min at room temperature and the mixture was reacted into hydrothermal autoclave at 150 °C for 72 h. The obtained material was washed with H_2O and filtered off. This washed material was suspended in 500 mL of HCl aqueous solution at pH 2 and stirred for 24 h. HCl treatment was repeated 3 times in order to remove the residual Na ions. After the HCl treatment, the suspension was centrifuged in order to separate the nanocatalyst from the solution [21].

2.3. Characterization

Infrared spectra of all samples were performed in KBr pellets in the 4000–400 cm^{-1} region with a resolution of 4 cm^{-1}, by accumulating 64 scans using a MB-100 Bomem FT-IR spectrophotometer.

FT-Raman spectra of the solid samples were obtained on a Brucker Equinox 55 equipped with a Raman accessory. The resulting spectra were the sum of 128 scans and the laser power was set to 200 mW with spectral resolution of 4 cm^{-1}.

Powder X-ray diffraction patterns were measured on a Brucker D8 Focus diffractometer using Cu Kα radiation. All the samples were scanned in the 2θ range of 2–50° at a scan rate of 2° min^{-1}.

Surface area was calculated by the Brunauer–Emmett–Teller (BET) method from nitrogen adsorption–desorption data, which was measured on a Quantachrome Nova 2200 analyzer.

Scanning electron microscopy (SEM) was performed on a Zeiss EVO 50 microscope. Samples were coated with carbon using a metalliser Baltec SCD 50. Apparatus was operated at 20 keV.

Surface charge density of TiO_2 catalyst as function of pH was calculated by using K_1 and K_2 values obtained from the simultaneous potentiometric and conductimetric titrations [20,22]. These titrations were carried out by using 50.0 mL of TiO_2 nanotubes aqueous suspension 40.0 g L^{-1}. Firstly, the TiO_2 nanotubes were fully deprotonated by adding of 0.4 mL of NaOH 1.0 mol L^{-1}. This sample was titrated with HNO_3 0.1 mol L^{-1}. The potentiometric readings were done by using a pHmeter pHTEK PHS-3B and the conductivity was measured by means of a Cole Parmer conductometer.

2.4. Malachite green photocatalytic degradation

The photodegradation of malachite green dye was carried out in a homemade photo-reactor [23,24] using 100.0 mL of a 5×10^{-5} mol L^{-1} dye solution and 0.1 g L^{-1} of the catalysts TiO_2 nanotubes and TiO_2 anatase. These solutions were illuminated by a mercury vapor lamp 125 W and the temperature was monitored during the reaction. The irradiation intensity per time was monitored by an Instrutherm UV-MRU-201 radiometer, which was 15 J cm^{-2} during 3 h of experiment. The dye degradation was followed on a Beckman DU-650 UV–Vis spectrophotometer.

2.5. pH effect

100.0 mL of a 5×10^{-5} mol L^{-1} of dye solution and TiO_2 nanotubes 0.1 g L^{-1} were applied to degrade malachite green dye 1.0×10^{-5} mol L^{-1} at different pH values, which were adjusted by the addition of HCl or NaOH solutions. The irradiation in the photoreactor was carried out during 60 min.

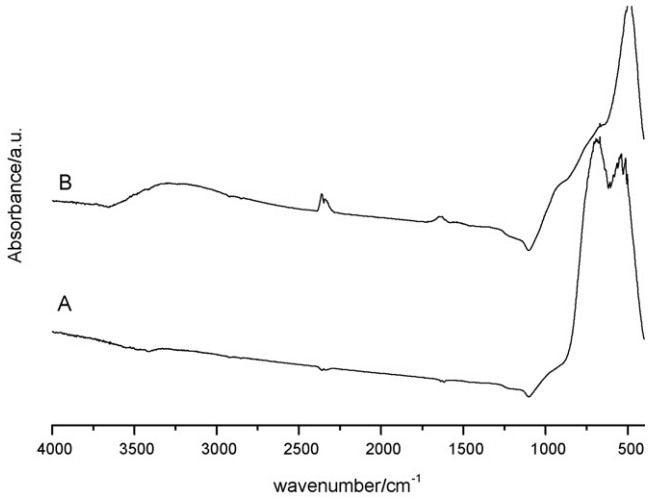

Fig. 1. FT-IR spectra of the TiO_2 anatase (A) and titania nanotubes (B).

2.6. Recycling of TiO_2 nanotubes compared with TiO_2 anatase

After malachite green photodegradation, the catalysts were filtrated and washed with water. Then, they were added to a photoreactor to be reused in another malachite green dye solution, in order to perform the same photodegradation.

3. Results and discussion

3.1. Characterization

FT-IR spectra (Fig. 1) shows some characteristic peaks of the catalysts such as: O–H stretching peak at 3300 cm^{-1} assigned to residual water and Ti–OH surface sites and a peak at 1640 cm^{-1} related to H–O–H bending mode. One peak at 930 cm^{-1} can also be observed, which is assigned to Ti–O–Ti bending mode and the peak at 490 cm^{-1} is related to Ti–OH stretching of surface materials [24–27].

Raman spectra of the precursor TiO_2 and titania nanotubes are presented in Fig. 2. Precursor TiO_2 spectrum presented only peaks related to the anatase phase at 141.7, 195.7, 396.2, 515.8 and 639.3 cm^{-1} [28,29]. Fig. 2B also showed peaks assigned to anatase phase of the nanotubes at 153.2, 191.8, 605.6 and 671.3 cm^{-1} [28,29]. However, this spectrum showed other characteristic peaks of nanotubular structure at 269.0, 446.4 and 671.3 cm^{-1} [30,31]. The bands at 446.4 peak were assigned to a pure framework Ti–O–Ti vibration of rutile phase and the peaks at 269.0 and 671.3 cm^{-1} were assigned to the Ti–O–H bonds in the interlayer regions of nanotube walls of rutile phase [30–34].

XRD patterns are presented in Fig. 3. Precursor TiO_2 presented a broad diffractions at $2\theta = 25$, 37, 38, 39, 48, 54, 55, 63, 69, 70 and 75 related to anatase structure (Fig. 3A). On the other hand, TiO_2 nanotubes also showed diffractions of anatase phase at $2\theta = 25$ and 49. Besides anatase peaks, one diffraction at $2\theta = 45$ related to rutile phase was observed (Fig. 3B). Characteristic peaks of the nanotube formation at $2\theta = 10$, 31 and 61 related to $H_2Ti_3O_7$ were also observed [31,33–35].

Fig. 4 shows the N_2 isotherm of adsorption for TiO_2 anatase (Fig. 4A) and TiO_2 nanotubes (Fig. 4B). The isotherm of TiO_2 anatase shows that the adsorption–desorption processes are reversible,

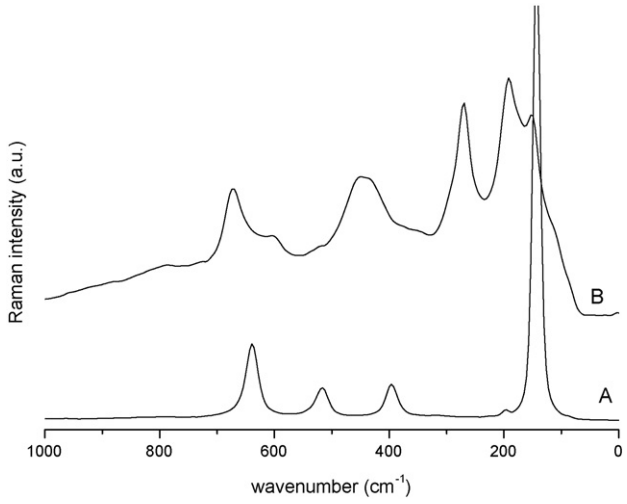

Fig. 2. FT-Raman spectra of the TiO_2 anatase (A) and titania nanotubes (B).

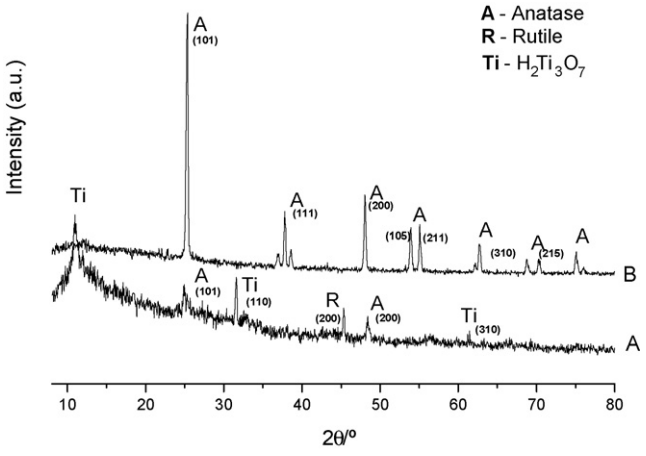

Fig. 3. XRD patterns for TiO_2 nanotubes (A) and TiO_2 anatase (B).

which is a typical characteristic of microporous material. On the other hand, this material presented a small hysteresis loop in the P/P_o range of 0.8–1.0, showing that the adsorption–desorption process is not reversible. This irreversibility is a consequence of capillary condensation in mesopores. Indeed, this isotherm shows that the TiO_2 nanotubes are predominantly formed by micropores with mesoporous sites forming an agglomerate structure [36–38]. The surface area values of catalysts were calculated by the application of BET equation in N_2 isotherms, which gave 8.0 and 76.0 $m^2\,g^{-1}$ for TiO_2 anatase and TiO_2 nanotubes, respectively. This fact proves that the formation of nanotubes from TiO_2 anatase causes a significant increase on the surface area of the material, which is one of the new qualities of this nanocatalyst when it is compared with the start material.

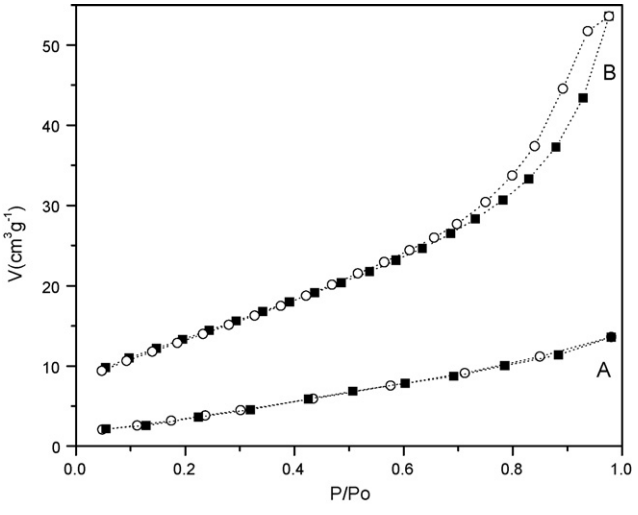

Fig. 4. Nitrogen adsorption–desorption isotherm for TiO_2 anatase (A) and TiO_2 nanotubes (B). Adsorption (■) and desorption (○) curves.

SEM images (Fig. 5) were carried out in order to understand the morphology of TiO_2 nanotubes, which shows that the TiO_2 nanotubes presented a diameter size of 20 nm.

The suspension of oxides in aqueous solution must form distinct surface charge sites as a result of two steps of protonation of the surface groups by hydration of the oxide surface leading to three distinct surface sites as according to Eqs. (1) and (2) [20,39].

$$MOH_2^+ \rightleftarrows MOH + H^+;\ K_1 \quad (1)$$

$$MOH \rightleftarrows MO^- + H^+;\ K_2 \quad (2)$$

The surface of this material is dependent on pH values, which can present an acidified surface (MOH_2^+) in strong acidic medium, amphoteric surface sites (MOH) in intermediate media, and basic surface sites (MO^-) in strong basic medium. The equilibrium constants K_1 and K_2 can be experimentally determined by the application of Henderson–Hasselbach equation in the simultaneous potentiometric and conductimetric titration data. From equilibrium constants, the surface charge density (σ) of TiO_2 nanotubes as function of pH values can be calculated by the application of Eq. (3) [20,40].

$$\rho_0 = \left(\frac{F}{A}\right)\left[\left(\frac{10^{-2pH} - K_1K_2}{10^{-2pH} + 10^{-pH}K_1 + K_1K_2}\right)N_T\right] \quad (3)$$

where F is the Faraday constant, A is the total surface area, N_T is the total number of moles of surface sites, and K_1 and K_2 correspond to the acid equilibria constants.

Fig. 6 was plotted by applying Eq. (3). This figure shows three distinct regions. The first region is assigned to the protonated surface corresponding to the MOH_2^+ acid sites up to pH 5.9 and 4.0 for TiO_2 anatase and TiO_2 nanotubes, respectively. TiO_2 anatase presented a small region of amphoteric surface sites (MOH) between pH 5.9 and 6.4, whereas TiO nanotubes presented a large amphoteric surface sites between pH 4.0 and 7.0. Above pH 6.4 and 7.0,

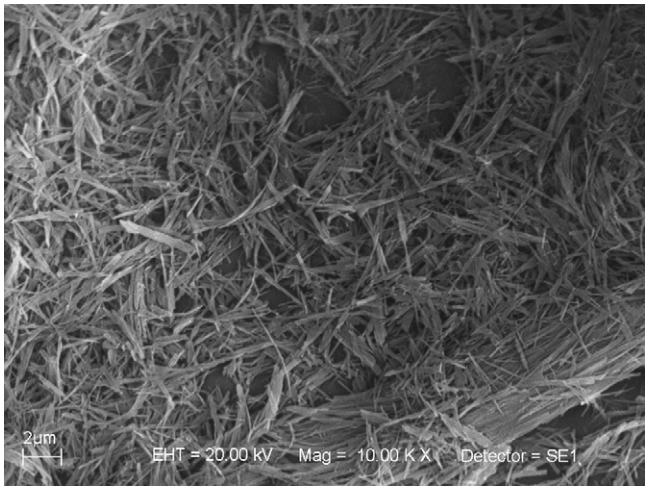

Fig. 5. SEM image of TiO_2 nanotubes.

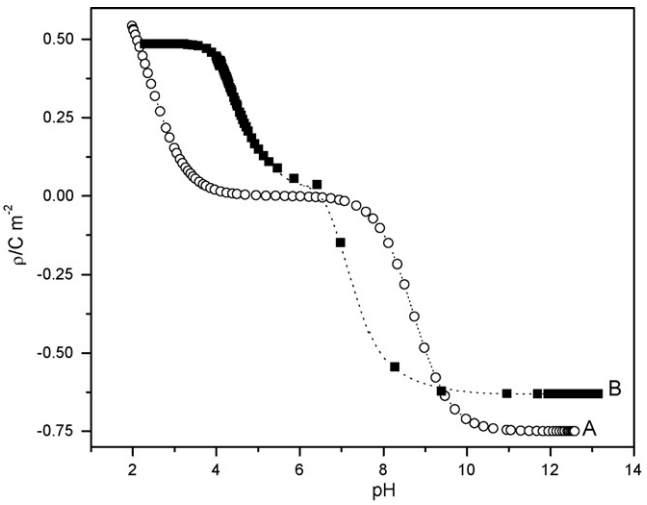

Fig. 6. Density surface charge as a function of pH for to TiO_2 anatase (■) and TiO_2 nanotubes (○).

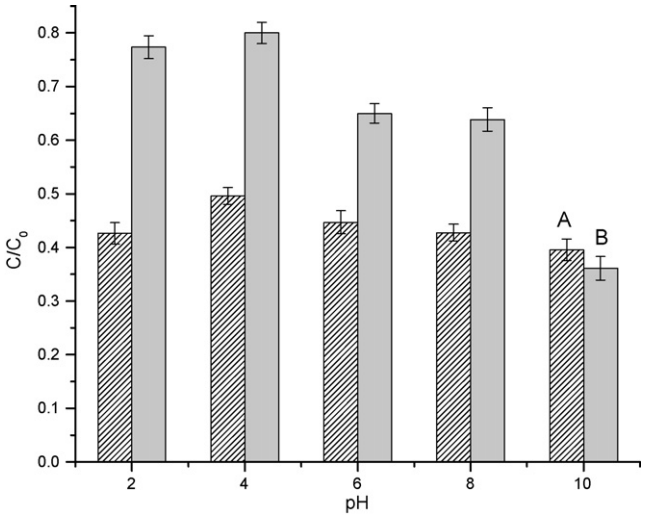

Fig. 8. The effect of pH value in photocatalytic activity of TiO_2 nanotubes (A) and TiO_2 anatase (B).

it can be observed the deprotonated (MO^-) surface sites for TiO_2 anatase and TiO_2 nanotubes, respectively. The point of zero charge (pzc) was observed at pH 6.2 and 5.6 for TiO_2 anatase and TiO_2 nanotubes, respectively.

3.2. Photocatalytic activity

The TiO_2 anatase is the main catalyst used in the contaminants photodegradation. However, the photocatalytic activity of TiO_2 nanotubes has not been developed so much according to the literature [41–43]. Thus, it is necessary a detailed study of the photocatalytic properties of TiO_2 nanotubes. In this way, the degradation of malachite green dye was followed as a function of time in the presence of TiO_2 nanotubes. This dye degradation was also followed in the presence of TiO_2 anatase in order to evaluate the photocatalytic ability of nanotubes in comparison with the key photocatalyst.

Fig. 7 shows that the TiO_2 presented a high photocatalytic activity to degrade malachite green, degrading practically 100% of dye at 75 min of reaction, whereas the TiO_2 nanotubes degraded the dye only at 105 min. These results showed that TiO_2 acts faster than TiO_2 nanotubes even taking into account that nanotubes present a surface area higher than TiO_2. This fact can be explained by the high stability of TiO_2 suspension in water, which increases the contact between contaminant and catalyst. Consequently, TiO_2 anatase presents photocatalytic an activity higher than TiO_2 nanotubes, which was according to the literature [43]. The effect of pH value in photocatalytic activity can be observed in Fig. 8.

The degradation was lower in basic medium for both catalysts. The degraded dye amount increases with the reduction of pH value. This behaviour suggests that the interaction between catalyst and dye must be occurred because of the interaction of acid sites MOH_2^+ or amphoteric sites MOH of catalysts with amine or aromatic groups of malachite green dye (Fig. 8). For both catalysts, the highest activity was observed at pH 4 and below this value their activities decreased. The addition of more acid in suspension at this pH must cause the increase of proton and chloride concentration, which can collapse the double layer to an extent that the ever-present attractive van der Waals forces overcome the charge repulsion [44]. As a consequence, the decrease of photocatalytic activity was observed in pH below 4.

The recycling studies were followed with TiO_2 anatase and TiO_2 nanotubes in order to compare their catalytic activities, as shown in Fig. 9. These studies revealed that TiO_2 recovery is difficult and

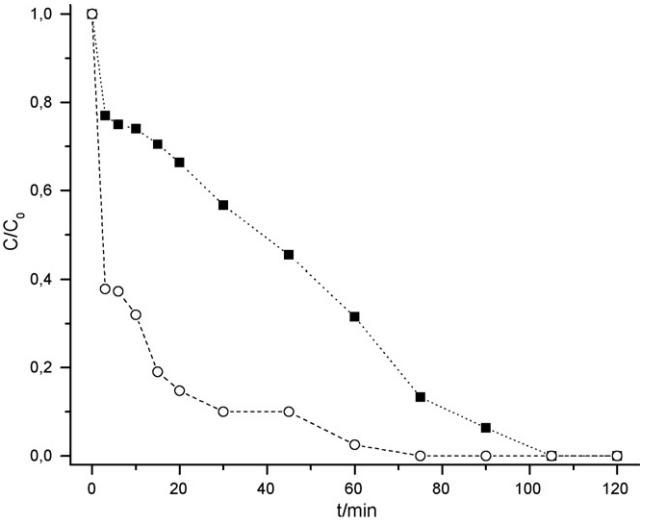

Fig. 7. Rates of photocatalysed degradation of the malachite green dye in the presence of TiO_2 anatase (○) and TiO_2 nanotubes (■).

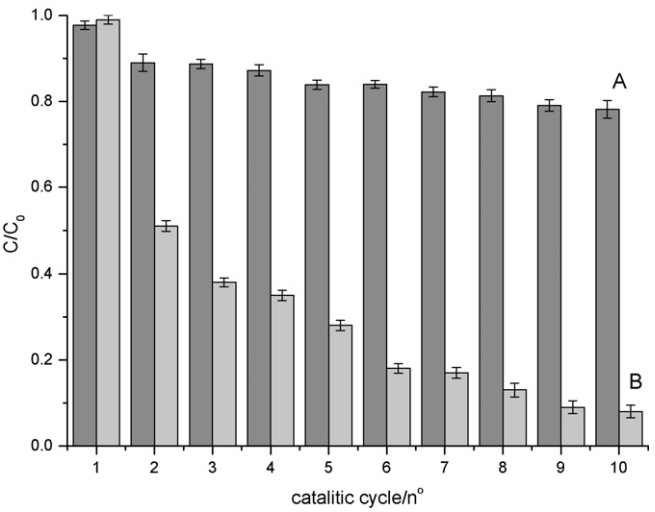

Fig. 9. Malachite green dye degradation for the recycling experiments of the TiO_2 nanotubes (A) and TiO_2 anatase photocatalysts (B).

the re-application of these catalysts is not effective. The high stability of TiO_2 anatase in aqueous medium, which generates a high photocatalytic activity, makes its separation from reaction solution difficult. The activity of TiO_2 anatase decreased dramatically to 8% of dye degradation after 10 catalytic cycles. On the other hand, TiO_2 nanotubes were easily recycled and maintained 80% of dye degradation after 10 catalytic cycles, showing the TiO_2 nanotubes ability to be reused in photodegradation reactions. The catalysis and the catalyst recovery to decrease contaminants from water are according to the key principles of green chemistry [45].

4. Conclusion

TiO_2 nanotubes presented a photocatalytic activity lower than TiO_2 anatase to degrade malachite green dye. The catalysts presented their best activity at pH 4. The great advantage of TiO_2 nanotubes is its easy recovery in comparison with traditional TiO_2 catalyst. Consequently, the nanotubes can be recycled and reapplied in many photodegradation cycles, maintaining 80% of their activity after 10 cycles of reaction. The precursor TiO_2 catalyst lost its activity on the second catalytic cycle.

Acknowledgments

The authors wish to thank FAPDF and CNPq for the financial support and CNPq and CAPES for the fellowships to AGSP and LLC.

References

[1] T. Robinson, G. McMullan, R. Marchant, P. Nigam, Remediation of dyes in textile effluent: a critical review on current treatment technologies with a proposed alternative, Biores. Technol. 77 (2001) 247–255.
[2] C.I. Pearce, J.R. Lloyd, J.T. Guthrie, The removal of colour from textile wastewater using whole bacterial cells: a review, Dyes Pigment 58 (2003) 179–196.
[3] A. Mahdavi Talarposhti, T. Donnelly, G.K. Anderson, Colour removal from a simulated dye wastewater using a two-phase anaerobic packed bed reactor, Water. Res. 35 (2001) 425–432.
[4] A.B. dos Santos, F.J. Cervantes, J.B. van Lier, Review paper on current technologies for decolourisation of textile wastewaters: perspectives for anaerobic biotechnology, Biores. Technol. 98 (2007) 2369–2385.
[5] A.G.S. Prado, J.D. Torres, E.A. Faria, S.C.L. Dias, Comparative adsorption studies of indigo carmine dye on chitin and chitosan, J. Colloid Interface Sci. 277 (2004) 43–47.
[6] M.S. Chiou, H.Y. Li, Equilibrium and kinetic modeling of adsorption of reactive dye on cross-linked chitosan beads, J. Hazard. Mater. 93 (2002) 233–248.
[7] S. Srivastava, R. Sinha, D. Roy, Toxicological effects of malachite green, Aqua. Toxicol. 66 (2004) 319–329.
[8] W. Cheng, S.G. Wang, L. Lu, W.X. Gong, X.W. Liu, B.Y. Gao, H.Y. Zhang, Removal of malachite green (MG) from aqueous solutions by native and heat-treated anaerobic granular sludge, Biochem. Eng. J. 39 (2008) 538–546.
[9] S.J. Culp, F.A. Beland, Malachite green: a toxicological review, J. Am. Coll. Toxicol. 15 (1996) 219–238.
[10] C.C. Chen, C.S. Lu, Y.C. Chung, J.L. Jan, UV light induced photodegradation of malachite green on TiO_2 nanoparticles, J. Hazard. Mater. 141 (2007) 520–528.
[11] I.A. Rahman, B. Saad, S. Shaidan, E.S. Sya Rizal, Adsorption characteristics of malachite green on activated carbon derived from rice husks produced by chemical–thermal process, Biores. Technol. 96 (2005) 1578–1583.
[12] Z. Bekçi, C. Ozveri, Y. Seki, K. Yurdakoç, Sorption of malachite green on chitosan bead, J. Hazard. Mater. 154 (2008) 254–261.
[13] L.A. Perez-Estrada, A. Aguera, M.D. Hernando, S. Malato, A.R. Fernandez Alba, Photodegradation of malachite green under natural sunlight irradiation: kinetic and toxicity of the transformation products, Chemosphere 70 (2008) 2068–2075.
[14] J.K. Lee, J.H. Gu, M.R. Kim, H.S. Chun, Incineration characteristics of dye sludge in a fluidized bed incinerator, J. Chem. Eng. Jpn. 34 (2001) 171–175.
[15] J. Garcia-Montano, X. Domenech, J.A. Garcia-Hortal, F. Torrades, P. Peral, The testing of several biological and chemical coupled treatments for Cibacron Red FN-R azo dye removal, J. Hazard. Mater. 154 (2008) 484–490.
[16] W. Chu, C.W. Ma, Quantitative prediction of direct and indirect dye ozonation kinetics, Water Res. 34 (2000) 3153–3160.
[17] A.G.S. Prado, B.M. Santos, G.V.M. Jacintho, Interaction of índigo carmine dye with sílica modified with humic acid at solid/liquid interface, Surf. Sci. 543 (2003) 276–282.
[18] A.G.S. Prado, E.A. Faria, J.R. SouzaDe, J.D. Torres, Ammonium complex of niobium as a precursor for the hydrothermal preparation of cellulose acetate/Nb_2O_5 photocatalyst, J. Mol. Catal. A 237 (2005) 115–119.
[19] J.D. Torres, E.A. Faria, J.R. SouzaDe, A.G.S. Prado, Preparation of photoactive chitosan–niobium (V) oxide composites for dye degradation, J. Photochem. Photobiol. A 182 (2006) 202–206.
[20] A.G.S. Prado, L.B. Bolzon, C.P. Pedroso, A.O. Moura, L.L. Costa, Nb_2O_5 as efficient and recyclable photocatalyst for indigo carmine degradation, Appl. Catal. B 82 (2008) 219–224.
[21] T. Kasuga, M. Hiramatsu, A. Hoson, T. Sekino, K. Niihara, Formation of titanium oxide nanotube, Langmuir 14 (1998) 3160–3163.
[22] N. Kallay, T. Madic, K. Kucej, T. Preocanin, Enthalpy of interfacial reactions at TiO_2 aqueous interface, Colloid. Surf. A 230 (2003) 3–11.
[23] E. DeOliveira, C.R. Neri, A.O. Ribeiro, V.S. Garcia, L.L. Costa, A.O. Moura, A.G.S. Prado, O.A. Serra, Y. Iamamoto, Hexagonal mesoporous silica modified with copper phthalocyanine as a photocatalyst for pesticide 2,4-dichlorophenoxiacetic acid degradation, J. Colloid Interface Sci. 323 (2008) 98–104.
[24] J. Zhu, D. Yang, J. Geng, D. Chen, Z. Jiang, Synthesis and characterization of bamboo-like CdS/TiO_2 nanotubes composites with enhanced visible-light photocatalytic activity, J. Nanopart. Res. 10 (2008) 729–736.
[25] T. Kasuga, M. Hiramatsu, A. Hoson, T. Sekino, K. Niihara, Titania nanotubes prepared by chemical processing, Adv. Mater. 11 (1999) 1307–1311.
[26] V.M. Cristante, A.G.S. Prado, S.M.A. Jorge, J.P.S. Valente, A.O. Florentino, P.M. Padilha, Synthesis and characterization of TiO_2 chemically modified by Pd(II) 2-aminothiazole complex for the photocatalytic degradation of phenol, J. Photochem. Photobiol. A 195 (2008) 23–29.
[27] T. Liu, F. Li, X. Li, TiO_2 hydrosols with high activity for photocatalytic degradation of formaldehyde in a gaseous phase, J. Hazard. Mater. 152 (2008) 347–355.
[28] P.T. Hsiao, K.P. Wang, C.W. Cheng, H.S. Teng, J. Nanocrystalline anatase TiO_2 derived from a titanate-directed route for dye-sensitized solar cells, J. Photochem. Photobiol. A 188 (2007) 19–24.
[29] L. Qian, Z.L. Du, S.Y. Yang, Z.S. Jin, Raman study of titania nanotube by soft chemical process, J. Mol. Struct. 749 (2005) 103–107.
[30] J.A. Toledo-Antonio, S. Capula, M.A. Cortes-Jacome, C. Angeles-Chavez, E. Lopez-Salinas, G. Ferrat, J. Navarrete, J. Escobar, Low-temperature FTIR study of CO adsorption on titania nanotubes, J. Phys. Chem. C 111 (2007) 10799–10805.
[31] M.A. Cortes-Jacome, G. Ferrat-Torres, L.F.F. Ortiz, C. Angeles-Chavez, E. Lopez-Salinas, J. Escobar, M.L. Mosqueira, J.A. Toledo-Antonio, In situ thermo-Raman study of titanium oxide nanotubes, Catal. Today 126 (2007) 248–255.
[32] M. Hodos, E. Horvath, H. Haspel, A. Kukovecz, Z. Konya, I. Kiricsi, Photo sensitization of ion-exchangeable titanate nanotubes by CdS nanoparticles, Chem. Phys. Lett. 399 (2004) 512–515.
[33] A. Kukovecz, M. Hodos, Z. Konya, I. Kiricsi, Complex-assisted one-step synthesis of ion-exchangeable titanate nanotubes decorated with CdS nanoparticles, Chem. Phys. Lett. 411 (2005) 445–449.
[34] D.V. Bavykin, J.M. Friedrich, A.A. Lapkin, F.C. Walsh, Stability of aqueous suspensions of titanate nanotubes, Chem. Mater. 18 (2006) 1124–1129.
[35] E. Horvath, A. Kukovecz, Z. Konya, I. Kiricsi, Hydrothermal conversion of self-assembled titanate nanotubes into nanowires in a revolving autoclave, Chem. Mater. 19 (2007) 927–931.
[36] E. DeOliveira, A.G.S. Prado, Ethylenediamine attached to sílica as an efficient, reusable, nanocatalyst for the addition of nitromethane to cyclopentenone, J. Mol. Catal. A 271 (2007) 63–69.
[37] P. Klobes, H. Preiss, K. Meyer, D. Shultze, Pore formation during the pyrolysis of C–Nb_2O_5 and C–Ta_2O_5 xerogels, Mikrochim. Acta 125 (1997) 343–347.
[38] E. DeOliveira, C.R. Neri, O.A. Serra, A.G.S. Prado, Antenna effect in highly luminescent Eu^{3+} anchored on hexagonal mesoporous silica, Chem. Mater. 19 (2007) 5437–5442.
[39] T. Preocanin, N. Kallay, Point of zero charge and surface charge density of TiO_2 in aqueous electrolyte solution as obtained by potentiometric mass titration, Croat. Chem. Acta 79 (2006) 95–106.
[40] A.F.C. Campos, F.A. Tourinho, G.J. da Silva, M.C.F.L. Lara, J. Depeyrot, Nanoparticles superficial density of charge in electric double-layered magnetic fluid: a conductimetric and potentiometric approach, Eur. Phys. J. E 6 (2001) 29–35.
[41] C.A. Grimes, Synthesis and application of highly ordered arrays of TiO_2 nanotubes, J. Mater. Chem. 17 (2007) 1451–1457.
[42] D.V. Bavykin, V.N. Parmon, A.A. Lapkin, F.C. Walsh, The effect of hydrothermal conditions on the mesoporous structure of TiO_2 nanotubes, J. Mater. Chem. 14 (2004) 3370–3377.
[43] Y.X. Yu, D.S. Xu, Single-crystalline TiO_2 nanorods: highly active and easily recycled photocatalysts, Appl. Catal. B 73 (2007) 166–171.
[44] W. Stumm, J.J. Morgan, Aquatic Chemistry: An Introduction Emphasizing Chemical Equilibria in Natural Waters, John Wiley & Sons, New York, 1981.
[45] A.G.S. Prado, Green chemistry, the chemical challenges of the new millennium, Quim. Nova 26 (2003) 738–744.